molecules

MDPI

*Article*

# Controlling the Treatment Time for Ideal Morphology towards Efficient Organic Solar Cells

**Yiwen Hou [1,†], Qiuning Wang [2,†], Ciyuan Huang [3,†], Tao Yang [1,*], Shasha Shi [3], Shangfei Yao [3], Donglou Ren [3,*], Tao Liu [3,*], Guangye Zhang [2,*] and Bingsuo Zou [3,*]**

1 Julong College, Shenzhen Technology University, Shenzhen 518118, China
2 College of New Materials and New Energies, Shenzhen Technology University, Shenzhen 518118, China
3 Guangxi Key Lab. of Processing for Nonferrous Metals and Featured Materials and Key Lab. of New Processing Technology for Nonferrous Metals and Materials, Ministry of Education, School of Resources, Environments and Materials, Guangxi University, Nanning 530004, China
* Correspondence: yangtao@sztu.edu.cn (T.Y.); rendonglou@gxu.edu.cn (D.R.); liutaozhx@gxu.edu.cn (T.L.); zhangguangye@sztu.edu.cn (G.Z.); zoubs@gxu.edu.cn (B.Z.)
† These authors contributed equally to this work. Order of authors was decided alphabetically.

**Abstract:** In this work, we performed a systematic comparison of different duration of solvent vapor annealing (SVA) treatment upon state-of-the-art PM6:SY1 blend film, which is to say for the first time, the insufficient, appropriate, and over-treatment's effect on the active layer is investigated. The power conversion efficiency (PCE) of corresponding organic solar cell (OSC) devices is up to 17.57% for the optimized system, surpassing the two counterparts. The properly tuned phase separation and formed interpenetrating network plays an important role in achieving high efficiency, which is also well-discussed by the morphological characterizations and understanding of device physics. Specifically, these improvements result in enhanced charge generation, transport, and collection. This work is of importance due to correlating post-treatment delicacy, thin-film morphology, and device performance in a decent way.

**Keywords:** solvent vapor annealing; power conversion efficiency; organic solar cell; morphology



**Citation:** Hou, Y.; Wang, Q.; Huang, C.; Yang, T.; Shi, S.; Yao, S.; Ren, D.; Liu, T.; Zhang, G.; Zou, B. Controlling the Treatment Time for Ideal Morphology towards Efficient Organic Solar Cells. *Molecules* **2022**, *27*, 5713. https://doi.org/10.3390/molecules27175713

Academic Editor: Elias Stathatos

Received: 17 August 2022
Accepted: 2 September 2022
Published: 5 September 2022



## 1. Introduction

Organic solar cell (OSC) technology is one of the most promising photovoltaics (PVs) to be commercialized, which can address the energy consumption issue without causing carbon oxide emission, eventually contributing to carbon neutralization [1–10]. To date, the urgent task for OSC researchers is to improve the power conversion efficiency (PCE) to a more competitive level, though it has been widely reported with > 18% [11–25]; the inputs of chemistry design/synthesis or ternary blend construction are unavoidable, yet the field demands a simple and effective way to improve the device efficiency based on mature material systems.

The eternal topic of improving the PCE involves realizing an ideal active layer morphology that is simultaneously favorable to charge generation, transport, and collection [26–34]. To do so, post-treatment on the active layer has been proven effective and promising [35–39]. For instance, Liu et al. reported three types of film morphology that cast layers treated in three different ways: no anneal, thermal anneal, and solvent vapor anneal, where solvent vapor anneal enabled type III morphology realized the highest PCE, due to the best charge generation producing the highest short-circuit current density ($J_{SC}$) [40]. Meanwhile, a large number of works have reported that solvent vapor annealing is effective to achieving ideal morphology for different types of blend films [41–47]. These results all suggest that solvent vapor annealing can induce favorable morphology under proper conditions, which is able to realize high PCE. However, for a high-efficiency system composed by polymer donor small molecular acceptors, the solvent vapor time has been rarely discussed, leaving

understanding blank for the field. Motivated by this inconspicuous blind spot, we plan to provide some insights on solvent fumigation duration's impact to OSC performance.

In this work, we carefully compared the effect of different solvent vapor annealing (SVA) times on active layer morphology and the device performance for a well-developed high-efficiency polymer donor small molecular acceptor composed binary blend, called PM6:SY1 [48]. The results show that with 30 s SVA by chloroform (CF), the active layer can produce the best PCE for OSCs, compared with its 0 s and 50 s counterparts (the operation mode is drawn in Figure 1). The efficiency enhancement comes from concurrently increased $J_{SC}$ and fill factor (*FF*), and the kept open-circuit voltage ($V_{OC}$). The overly annealed film suffers PCE loss due to the decrease in $J_{SC}$ and *FF*. The morphology characterization reveals that the properly fumigated active layer has a better interpenetrating network and slightly reduced phase separation, which facilitates the charge transport. The 50-s SVA-treated film has similar network, but much increased pure domain size; thus, it has overly purified phase distribution and poorer charge generation. The device physics investigation confirms the guess, specifically, better charge generation, transport, and collection. The best efficiency (17.57%) here is at the same level reported recently in some high-level journals using similar method and PM6 as donor [41]. This work successfully correlates the post-treatment, thin-film morphology, and device efficiency, and is instructive for further realizing PCE progress of OSCs.

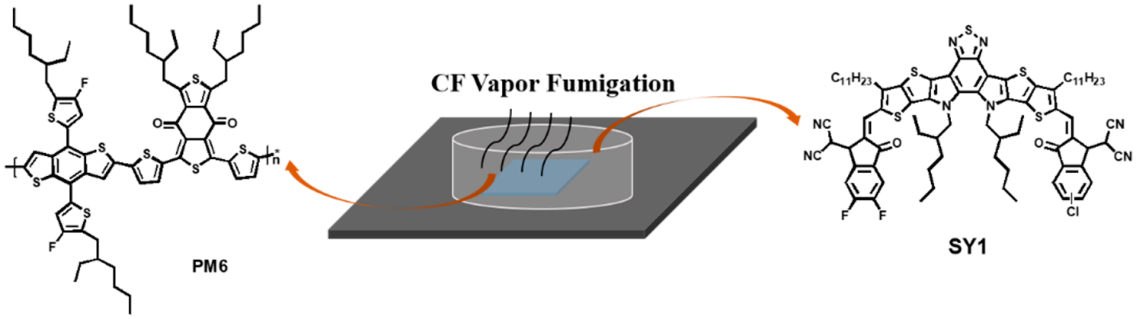


**Figure 1.** Schematic diagram of CF SVA-treated film based on PM6 and SY1.

## 2. Results and Discussion

The variation in blend film's ultraviolet–visible (UV–vis) absorption, a basic optical property and reflection of aggregation change, is presented in Figure 2a. Proper treatment duration (30 s) can rationally improve the absorbance of the film, indicating that ideal morphology is achieved. When the time elongates to 50 s, the absorbance generally drops, especially the donor part, implying unfavorable destruction of PM6's network. As for 80 s, the absorbance of acceptor rises to an extremely high level such that over-phase-purification happens while the PM6's network is indicated to be seriously harmed.

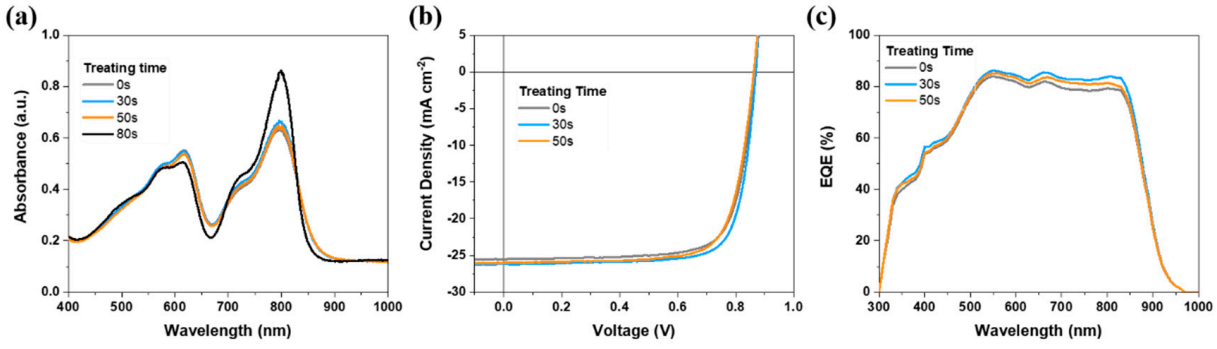


**Figure 2.** (**a**) UV–vis absorption of active layers. (**b**) *J*–*V* characteristics. (**c**) EQE spectra.

A series of devices based on traditional structures ITO/PEDOT:PSS-TA/PM6:SY1 /PDINN/Ag were fabricated to investigate the photovoltaic parameter change [49,50]. The optimal device performances of each kind of treated film are illustrated as the form of current density vs. voltage (*J*–*V*) characteristics in Figure 2b, and details of photovoltaic parameters are summarized in Table 1. The control device without SVA treatment has a moderate $J_{SC}$ of 25.49 mA cm$^{-2}$ and an *FF* of 75.7%. The 30-s chloroform (CF)-fumigated active layer enabled OSC presented a clearly improved $J_{SC}$ of 26.14 mA cm$^{-2}$ and *FF* of 77.4%, which is responsible for the optimized PCE of 17.57%. When the SVA treatment time prolongs to 50 s, the device efficiency drops to 16.80%, where the $J_{SC}$ and *FF* turn back to a lower level. The 20 independent device data are given in Table S1 for clear information. When the duration prolongs to 80 s, the efficiency drops to an even lower level, where the best PCE is only 15.51% (as shown in Figure S1 Supplementary material), due to the drop of $J_{SC}$ and *FF*. Furthermore, other two constantly used solvents for SVA are investigated and the results are given in Figure S2 for reference. Both tetrahydrofuran (THF) and chlorobenzene (CB) cannot appeal with CF.

**Table 1.** Device performances.

| PM6:SY1 | $V_{OC}$ (V) | $J_{SC}$ (mA cm$^{-2}$) | *FF* (%) | PCE (%) |
|---|---|---|---|---|
| SVA 0 s | 0.865 | 25.49/25.89 | 75.7 | 16.69 (16.44 ± 0.17) |
| SVA 30 s | 0.869 | 26.14/25.93 | 77.4 | 17.57 (17.30 ± 0.20) |
| SVA 50 s | 0.862 | 25.97/25.40 | 75.0 | 16.80 (16.60 ± 0.10) |
| SVA 80 s | 0.857 | 25.06/24.63 | 72.2 | 15.51 |

Integrated current density values are behind the slashes. The brackets contain averages and standard errors of PCEs based on at least 20 devices.

Then, we performed the external quantum efficiency (EQE) spectra measurement to check the accuracy of photovoltaic test. As shown in Figure 2c and the integrated value in Table 1, the errors are well-controlled within 3%. The profiles suggests that general charge generation is enhanced for SVA treatment devices, though the overly fumigated one suffers some loss compared with the optimal target.

The morphology understanding, specifically for the SVA-induced phase separation, is enabled by using the atomic force spectroscopy (AFM) measurement and the grazing incidence small-angle X-ray scattering (GISAXS) test [51–55]. The results are displayed in Figure 3. According to the height images, the surface roughness determined by the root mean square (RMS) values for them are 1.63 nm, 1.15 nm, and 1.23 nm, respectively. This is to say that SVA treatment can reduce the aggregation of materials, which is supposed to be beneficial to charge collection at interface and charge generation. Meanwhile, the phase images show that SVA processing helps the formation of interpenetrating nanostructure, a typical favorable morphology feature for OSCs [56–59]. These results indicate that SVA treatment bears the hope of boosting $J_{SC}$ and *FF*. Then, the difference between the treatment time is compared by the fitted GISAXS results. The pure acceptor phase sizes of them are 31.2 nm, 27.5 nm, and 38.3 nm. The reduced domain size of optimally fumigated film is consistent with better charge generation, and its overlay version shows the largest domain size, which is considered harmful to maintaining $J_{SC}$ and *FF*, since the recrystallization process and phase purification overwhelmingly happened [35].

Then, we return our attention to device physics to connect the morphology observation and device performances. The efficiencies of charge generation and collection are evaluated by photocurrent density vs. effective ($J_{ph}$ vs. $V_{eff}$) relationships, as drawn in Figure 4a. As a result, charge generations for 0 s, 30 s, and 50 s SVA-treated devices are 92.1%, 93.2%, and 91.7%; meanwhile, the collection efficiencies are 84.5%, 87.1%, and 83.5%, respectively. The trap-assisted recombination and bimolecular recombination change of the devices are studied by the $V_{OC}$ and $J_{SC}$ vs. light intensity relationships, as given in Figure 4b,c. The fitted ideal factors are 1.18, 1.05, and 1.22, respectively. Additionally, the bimolecular recombination rates are found to be 0.97, 0.98, and 0.96. These results show that, when

pretreated by SVA properly, the recombination can be well-suppressed, which is beneficial to $J_{SC}$ and *FF*.

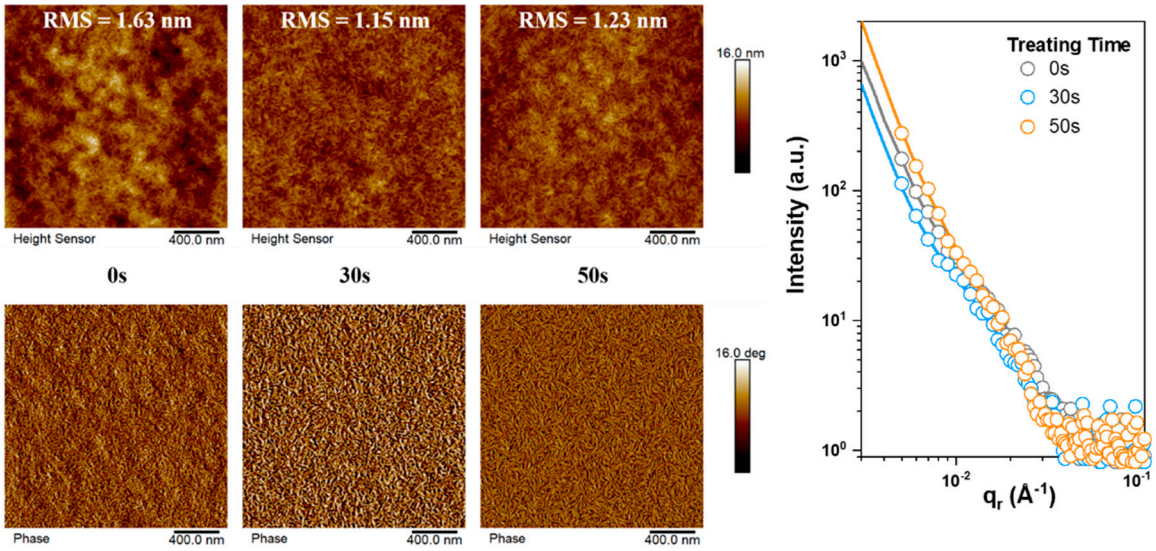


**Figure 3.** AFM height and phase images, and GISAXS results.

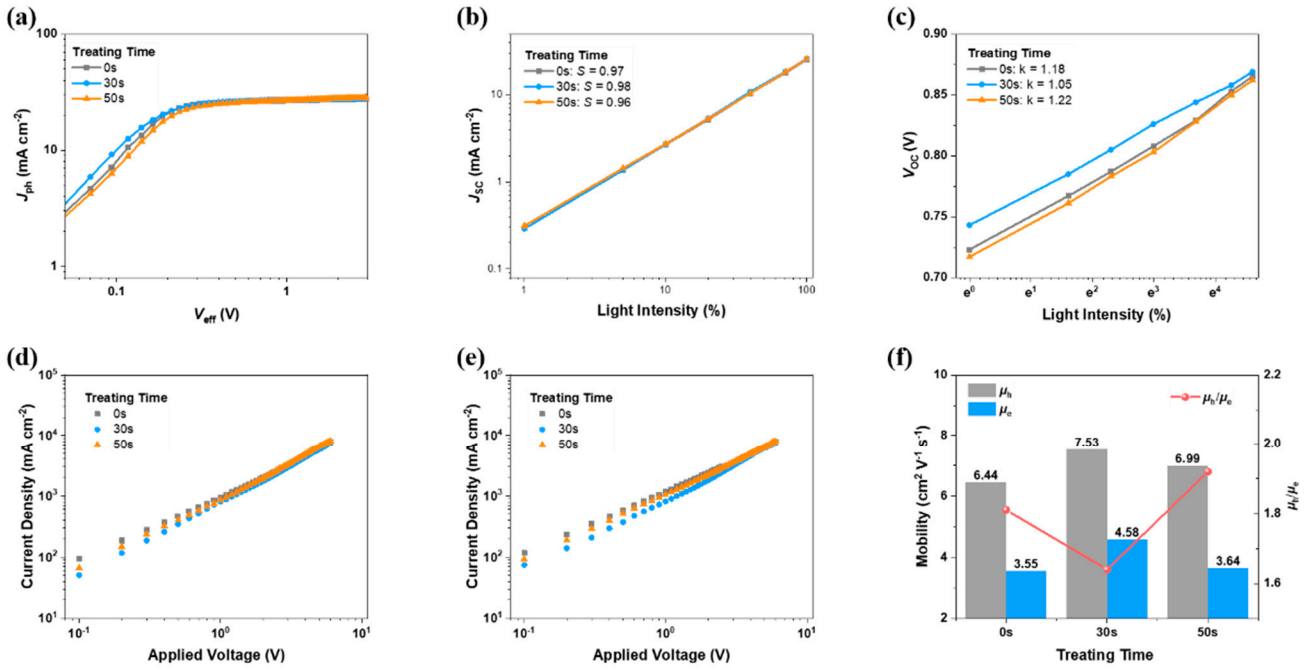


**Figure 4.** (**a**) $J_{ph}$ vs. $V_{eff}$ relationships. (**b**) $J_{SC}$ and (**c**) $V_{OC}$ vs. light intensity plots. Hole-only (**d**) and electron-only (**e**) device results. (**f**) summarized $\mu_h$, $\mu_e$ and ratios.

Furthermore, the charge transport improvement is expected to be confirmed, by using the space-charge limited current (SCLC) method. The results of hole-only and electron-only devices are shown in Figure 4d,e, where the linear relationship of applied voltage and squared current density is determined. The calculated hole and electron mobilities ($\mu_h$, $\mu_e$), together with the $\mu_h/\mu_e$ ratios, are presented in Figure 2f. It is found that optimal film has the most efficient and balanced charge transport, which facilitates the pursuit of *FF*.

## 3. Materials and Methods

### *3.1. Characterization*

AFM measurements were obtained by using a Dimension Icon AFM (Bruker, Billerica, MA, USA) in tapping mode. The grazing incidence X-ray scattering (GIWAXS) measurement was carried out with a Xeuss 2.0 SAXS/WAXS laboratory beamline using a Cu X-ray source (8.05 keV, 1.54 Å) and a Pilatus3R 300 K detector. The incident angle was 0.2°. The samples for GISAXS measurements were fabricated on silicon substrates using the same recipe for the devices.

### *3.2. Solar Cell Fabrication and Characterization*

Solar cells were fabricated in a conventional device configuration of ITO/PEDOT:PSS-TA/active layers/PDINN/Ag. The ITO substrates were first scrubbed by detergent; then sonicated with deionized water, acetone, and isopropanol; and dried overnight in an oven. The glass substrates were treated by UV–Ozone for 30 min before use. PEDOT:PSS (Heraeus Clevios P VP AI 4083) doped by pyramine hydrochloride was spin-cast onto the ITO substrates at 4000 rpm for 30 s, and then dried at 150 °C for 15 min in air. The PM6:SY1 (1:1.2) was dissolved in 15 mg $mL^{-1}$ chloroform with 1-chloronaphthalene (0.5% vol) as additive and stirred overnight in a nitrogen-filled glove box. The solution was spin-cast at 3000 rpm for 30 s onto PEDOT:PSS-TA films followed by solvent vapor (saturated CF) annealing for different time. A thin PDINN layer was coated on the active layer, followed by the deposition of Ag (evaporated under $5 \times 10^{-4}$ Pa through a shadow mask). The optimal active layer thickness measured by a Bruker Dektak XT stylus profilometer (Bruker, Billerica, Massachusetts, United States) was about 100 nm. The current density–voltage (*J*–*V*) curves of all encapsulated devices (by Epoxy) were measured using a Keithley 2400 Source Meter in air under AM 1.5 G (100 mW $cm^{-2}$) using a Newport solar simulator, where the applied voltage varies from −1.3 V to 0.5 V. The light intensity was calibrated using a standard Si diode (with KG5 filter, purchased from PV Measurement to bring spectral mismatch to unity). The scan speed is about 0.5 V/s, and devices were scanned several times to exlude the effect of burn-in loss. Optical microscope (Olympus BX51, Shinjuku City, Tokyo) was used to define the device area (4.0 $mm^2$). EQEs were measured using an Enlitech QE-S EQE system equipped with a standard Si diode. Monochromatic light was generated from a Newport 300 W lamp source.

### *3.3. SCLC Measurements*

The electron and hole mobility were measured using the method of space-charge limited current (SCLC) for electron-only devices with the structure of ITO/ZnO/active layer/PDINN/Ag and ITO/PEDOT:PSS-TA/active layers/$MoO_x$/Ag for hole-only devices. The charge carrier mobility was determined by fitting the dark current to the model of a single-carrier SCLC according to the equation $J = 9\varepsilon_0\varepsilon_r\mu V^2/8d^3$, where $J$ is the current density, $d$ is the film thickness of the active layer, $\mu$ is the charge carrier mobility, $\varepsilon_r$ is the relative dielectric constant of the transport medium, and $\varepsilon_0$ is the permittivity of free space. $V = V_{app} - V_{bi}$, where $V_{app}$ is the applied voltage and $V_{bi}$ is the offset voltage. The carrier mobility can be calculated from the slope of the $J^{1/2}$~$V$ curves.

### *3.4. The Analysis of $J_{ph}$ vs. $V_{eff}$ Relationships*

The definition of $J_{ph}$ is the current density under illumination ($J_L$) minus the dark current density ($J_D$), and $V_0$ refers to the voltage value when $J_{ph} = 0$. Accordingly, $V_{eff} = V_0 - V_{appl}$, where $V_{appl}$ represents applied voltage, has a clear meaning. Importantly, when $V_{eff}$ reaches a high value (> 2V), it is normally believed that generated excitons are fully collected, in which $J_{ph}$ is equal to saturated current density ($J_{sat}$). Then, we can calculate $J_{SC}/J_{sat}$ and $J_{max}/J_{sat}$ to describe exciton dissociation ($\eta_{diss}$) and charge collection ($\eta_{coll}$) efficiency. $J_{max}$ is the $J_{ph}$ at the maximal output point.

## 4. Conclusions

In summary, the SVA treatment time is found to be impactful in determining the final morphology feature and device performances. Previous work demonstrated the effectiveness of SVA, but rarely paid attention to the processing time. Thereby, the work herein is meaningful for the field to understand how to realize high PCE. The best device efficiency, as high as 17.57%, was enabled by improved $J_{SC}$ and *FF*, and the other two counterparts suffered poorer performance due to unfavorable morphology features, where initially large phase separation was found to be the reason. The device physics investigation confirmed the guess, specifically, better charge generation, transport, and collection. This work is of importance due to correlating the post-treatment delicacy, thin-film morphology, and device performance in a decent way. Possible future works could lie in finding out more proper treating solvents and more suitable photovoltaic systems to achieve higher PCE and even break through the bottleneck of the whole field.

**Supplementary Materials:** The following supporting information can be downloaded at: https://www.mdpi.com/article/10.3390/molecules27175713/s1, Figure S1: *J-V* characteristics and EQE spectra for SVA 80s device; Figure S2: *J-V* characteristics and EQE spectra for THF and CB treated devices.; Table S1: Independent device results.

**Author Contributions:** Conceptualization, T.Y.; Data curation, Y.H. and T.L.; Formal analysis, Y.H., Q.W. and C.H.; Funding acquisition, D.R., G.Z. and B.Z.; Investigation, Y.H., C.H. and S.S.; Methodology, Q.W., S.Y., D.R. and G.Z.; Project administration, T.Y., G.Z. and B.Z.; Resources, D.R.; Supervision, T.Y., S.Y., T.L., G.Z. and B.Z.; Validation, C.H.; Writing–original draft, Y.H., Q.W. and C.H.; Writing–review & editing, G.Z. All authors have read and agreed to the published version of the manuscript.

**Funding:** T. Yang appreciates the Shenzhen Key Laboratory of Marine Energies and Environmental Safety (ZDSYS20201215154000001) and Shenzhen Overseas Talent Project (NO. GDRC202102), the project all-solid-state high energy density energy storage battery system (20221063010031), also thanks Shenzhen Key Laboratory of Marine.

**Institutional Review Board Statement:** Not applicable.

**Informed Consent Statement:** Not applicable.

**Data Availability Statement:** Data are available from authors based on reasonable requirement from readers.

**Acknowledgments:** Xinhui Lu of CUHK is appreciated for the help of morphology characterization. T. Yang appreciates the Shenzhen Key Laboratory of Marine Energies and Environmental Safety (ZDSYS20201215154000001) and Shenzhen Overseas Talent Project (NO. GDRC202102). B. Zou thanks the Guangxi NSF project (2020GXNSFDA238004) the Scientific and Technological Bases and Talents of Guangxi (Guike AD21238027), the special fund for "Guangxi Bagui Scholars". G. Zhang acknowledges the support by the Guangdong Basic and Applied Basic Research Foundation (2022A1515010875), Guangdong Basic and Applied Basic Research Foundation (2021A1515110017), Natural Science Foundation of Top Talent of SZTU (grant no. 20200205), Project of Education Commission of Guangdong Province of China (2021KQNCX080).

**Conflicts of Interest:** The authors declare no conflict of interest.

**Sample Availability:** Samples of the compounds are not available from the authors.

## References

1. Su, Y.-W.; Lan, S.-C.; Wei, K.-H. Organic photovoltaics. *Mater Today* **2012**, *15*, 554–562. [CrossRef]
2. Cui, C.; Li, Y. Morphology optimization of photoactive layers in organic solar cells. *Aggregate* **2021**, *2*, e31. [CrossRef]
3. Heeger, A.J. 25th Anniversary Article: Bulk Heterojunction Solar Cells: Understanding the Mechanism of Operation. *Adv. Mater.* **2014**, *26*, 10–28. [CrossRef] [PubMed]
4. Yang, C.; Zhang, S.; Hou, J. Low-cost and efficient organic solar cells based on polythiophene- and poly(thiophene vinylene)-related donors. *Aggregate* **2022**, e111. [CrossRef]
5. Ma, R.; Liu, T.; Luo, Z.; Guo, Q.; Xiao, Y.; Chen, Y.; Li, X.; Luo, S.; Lu, X.; Zhang, M.; et al. Improving open-circuit voltage by a chlorinated polymer donor endows binary organic solar cells efficiencies over 17%. *Sci. China Ser. B: Chem.* **2020**, *63*, 325–330. [CrossRef]

6. Yan, C.; Qin, J.; Wang, Y.; Li, G.; Cheng, P. Emerging Strategies toward Mechanically Robust Organic Photovoltaics: Focus on Active Layer. *Adv. Energy Mater.* **2022**, *12*, 2201087. [CrossRef]
7. Sun, H.; Guo, X.; Facchetti, A. High-Performance n-Type Polymer Semiconductors: Applications, Recent Development, and Challenges. *Chem* **2020**, *6*, 1310–1326. [CrossRef]
8. Ma, R.; Yang, T.; Xiao, Y.; Liu, T.; Zhang, G.; Luo, Z.; Li, G.; Lu, X.; Yan, H.; Tang, B. Air-Processed Efficient Organic Solar Cells from Aromatic Hydrocarbon Solvent without Solvent Additive or Post-Treatment: Insights into Solvent Effect on Morphology. *Energy Environ. Mater.* **2021**, *5*, 977–985. [CrossRef]
9. Ge, J.; Hong, L.; Song, W.; Xie, L.; Zhang, J.; Chen, Z.; Yu, K.; Peng, R.; Zhang, X.; Ge, Z. Solvent Annealing Enables 15.39% Efficiency All-Small-Molecule Solar Cells through Improved Molecule Interconnection and Reduced Non-Radiative Loss. *Adv. Energy Mater.* **2021**, *11*, 2100800. [CrossRef]
10. Ma, R.; Yu, J.; Liu, T.; Zhang, G.; Xiao, Y.; Luo, Z.; Chai, G.; Chen, Y.; Fan, Q.; Su, W.; et al. All-polymer solar cells with over 16% efficiency and enhanced stability enabled by compatible solvent and polymer additives. *Aggregate* **2022**, *3*, e58. [CrossRef]
11. Bao, S.; Yang, H.; Fan, H.; Zhang, J.; Wei, Z.; Cui, C.; Li, Y. Volatilizable Solid Additive-Assisted Treatment Enables Organic Solar Cells with Efficiency over 18.8% and Fill Factor Exceeding 80%. *Adv. Mater.* **2021**, *33*, 2105301. [CrossRef] [PubMed]
12. Ma, R.; Yan, C.; Fong, P.W.-K.; Yu, J.; Liu, H.; Yin, J.; Huang, J.; Lu, X.; Yan, H.; Li, G. In situ and ex situ investigations on ternary strategy and co-solvent effects towards high-efficiency organic solar cells. *Energy Environ. Sci.* **2022**, *15*, 2479–2488. [CrossRef]
13. Zuo, L.; Jo, S.B.; Li, Y.; Meng, Y.; Stoddard, R.J.; Liu, Y.; Lin, F.; Shi, X.; Liu, F.; Hillhouse, H.W.; et al. Dilution effect for highly efficient multiple-component organic solar cells. *Nat. Nanotechnol.* **2021**, *17*, 53–60. [CrossRef] [PubMed]
14. Zou, Y.; Chen, H.; Bi, X.; Xu, X.; Wang, H.; Lin, M.; Ma, Z.; Zhang, M.; Li, C.; Wan, X.; et al. Peripheral Halogenation Engineering Controls Molecular Stacking to Enable Highly Efficient Organic Solar Cells. *Energy Environ. Sci.* **2022**, *15*, 3519–3533. [CrossRef]
15. Luo, Z.; Ma, R.; Yu, J.; Liu, H.; Liu, T.; Ni, F.; Hu, J.; Zou, Y.; Zeng, A.; Su, C.-J.; et al. Heteroheptacene-based acceptors with thieno [3,2-b] pyrrole yield high-performance polymer solar cells. *Natl. Sci. Rev.* **2022**, *9*, nwac076. [CrossRef] [PubMed]
16. He, C.; Chen, Z.; Wang, T.; Shen, Z.; Li, Y.; Zhou, J.; Yu, J.; Fang, H.; Li, Y.; Li, S.; et al. Asymmetric electron acceptor enables highly luminescent organic solar cells with certified efficiency over 18%. *Nat. Commun.* **2022**, *13*, 2598. [CrossRef]
17. Xiong, X.; Xue, X.; Zhang, M.; Hao, T.; Han, Z.; Sun, Y.; Zhang, Y.; Liu, F.; Pei, S.; Zhu, L. Melamine-Doped Cathode Interlayer Enables High-Efficiency Organic Solar Cells. *ACS Energy Lett.* **2021**, *6*, 3582–3589. [CrossRef]
18. Zhan, L.; Li, S.; Li, Y.; Sun, R.; Min, J.; Bi, Z.; Ma, W.; Chen, Z.; Zhou, G.; Zhu, H.; et al. Desired open-circuit voltage increase enables efficiencies approaching 19% in symmetric-asymmetric molecule ternary organic pho-tovoltaics. *Joule* **2022**, *6*, 662–675. [CrossRef]
19. Yu, J.; Liu, X.; Zhong, Z.; Yan, C.; Liu, H.; Fong, P.W.; Liang, Q.; Lu, X.; Li, G. Copper phosphotungstate as low cost, solution-processed, stable inorganic anode interfacial material enables organic photovoltaics with over 18% efficiency. *Nano Energy* **2022**, *94*, 106923. [CrossRef]
20. Chen, S.; Feng, L.; Jia, T.; Jing, J.; Hu, Z.; Zhang, K.; Huang, F. High-performance polymer solar cells with efficiency over 18% enabled by asymmetric side chain engineering of non-fullerene acceptors. *Sci. China Ser. B Chem.* **2021**, *64*, 1192–1199. [CrossRef]
21. Cai, Y.; Li, Q.; Lu, G.; Ryu, H.S.; Li, Y.; Jin, H.; Chen, Z.; Tang, Z.; Lu, G.; Hao, X.; et al. Vertically optimized phase separation with improved exciton diffusion enables efficient organic solar cells with thick active layers. *Nat. Commun.* **2022**, *13*, 2369. [CrossRef]
22. Hong, L.; Yao, H.; Cui, Y.; Bi, P.; Zhang, T.; Cheng, Y.; Zu, Y.; Qin, J.; Yu, R.; Ge, Z.; et al. 18.5% Efficiency Organic Solar Cells with a Hybrid Planar/Bulk Heterojunction. *Adv. Mater.* **2021**, *33*, 2103091. [CrossRef]
23. Zhu, L.; Zhang, M.; Xu, J.; Li, C.; Yan, J.; Zhou, G.; Zhong, W.; Hao, T.; Song, J.; Xue, X.; et al. Single-junction organic solar cells with over 19% ef-ficiency enabled by a refined double-fibril network morphology. *Nat. Mater.* **2022**, *21*, 656–663. [CrossRef]
24. Cui, Y.; Xu, Y.; Yao, H.; Bi, P.; Hong, L.; Zhang, J.; Zu, Y.; Zhang, T.; Qin, J.; Ren, J.; et al. Single-Junction Organic Photovoltaic Cell with 19% Efficiency. *Adv. Mater.* **2021**, *33*, 2102420. [CrossRef]
25. Wei, Y.; Chen, Z.; Lu, G.; Yu, N.; Li, C.; Gao, J.; Gu, X.; Hao, X.; Lu, G.; Tang, Z.; et al. Binary Organic Solar Cells Breaking 19% via Manipulating the Vertical Component Distribution. *Adv. Mater.* **2022**, *34*, 2204718. [CrossRef]
26. Zhu, L.; Zhang, M.; Zhong, W.; Leng, S.; Zhou, G.; Zou, Y.; Su, X.; Ding, H.; Gu, P.; Liu, F.; et al. Progress and prospects of the morphology of non-fullerene acceptor based high-efficiency organic solar cells. *Energy Environ. Sci.* **2021**, *14*, 4341–4357. [CrossRef]
27. Naveed, H.B.; Ma, W. Miscibility-Driven Optimization of Nanostructures in Ternary Organic Solar Cells Using Non-fullerene Acceptors. *Joule* **2018**, *2*, 621–641. [CrossRef]
28. Zhao, F.; Wang, C.; Zhan, X. Morphology Control in Organic Solar Cells. *Adv. Energy Mater.* **2018**, *8*, 1703147. [CrossRef]
29. Kan, B.; Kan, Y.; Zuo, L.; Shi, X.; Gao, K. Recent progress on all-small molecule organic solar cells using small-molecule nonfullerene acceptors. *InfoMat* **2020**, *3*, 175–200. [CrossRef]
30. Zhou, K.; Xian, K.; Qi, Q.; Gao, M.; Peng, Z.; Liu, J.; Liu, Y.; Li, S.; Zhang, Y.; Geng, Y.; et al. Unraveling the Correlations between Mechanical Properties, Miscibility, and Film Microstructure in All-Polymer Photovoltaic Cells. *Adv. Funct. Mater.* **2022**, *32*, 2201781. [CrossRef]
31. Ma, R.; Zhou, K.; Sun, Y.; Liu, T.; Kan, Y.; Xiao, Y.; Dela Peña, T.A.; Li, Y.; Zou, X.; Xing, Z.; et al. Achieving high efficiency and well-kept ductility in ternary all-polymer organic photovoltaic blends thanks to two well miscible donors. *Matter* **2022**, *5*, 725–734. [CrossRef]

32. Ma, Y.; Zhang, M.; Wan, S.; Yin, P.; Wang, P.; Cai, D.; Liu, F.; Zheng, Q. Efficient Organic Solar Cells from Molecular Orientation Control of M-Series Acceptors. *Joule* **2021**, *5*, 197–209. [CrossRef]
33. Ma, R.; Tao, Y.; Chen, Y.; Liu, T.; Luo, Z.; Guo, Y.; Xiao, Y.; Fang, J.; Zhang, G.; Li, X.; et al. Achieving 16.68% efficiency ternary as-cast organic solar cells. *Sci. China Ser. B: Chem.* **2021**, *64*, 581–589. [CrossRef]
34. Xian, K.; Liu, Y.; Liu, J.; Yu, J.; Xing, Y.; Peng, Z.; Zhou, K.; Gao, M.; Zhao, W.; Lu, G.; et al. Delicate crystallinity control enables high-efficiency P3HT organic photovoltaic cells. *J. Mater. Chem. A* **2022**, *10*, 3418–3429. [CrossRef]
35. Gao, K.; Deng, W.; Xiao, L.; Hu, Q.; Kan, Y.; Chen, X.; Wang, C.; Huang, F.; Peng, J.; Wu, H.; et al. New insight of molecular interaction, crystallization and phase separation in higher performance small molecular solar cells via solvent vapor annealing. *Nano Energy* **2016**, *30*, 639–648. [CrossRef]
36. Gao, K.; Jo, S.B.; Shi, X.; Nian, L.; Zhang, M.; Kan, Y.; Lin, F.; Kan, B.; Xu, B.; Rong, Q.; et al. Over 12% Efficiency Nonfullerene All-Small-Molecule Organic Solar Cells with Sequentially Evolved Multilength Scale Morphologies. *Adv. Mater.* **2019**, *31*, e1807842. [CrossRef] [PubMed]
37. Ma, W.; Yang, C.; Gong, X.; Lee, K.; Heeger, A.J. Thermally Stable, Efficient Polymer Solar Cells with Nanoscale Control of the Interpenetrating Network Morphology. *Adv. Funct. Mater.* **2005**, *15*, 1617–1622. [CrossRef]
38. Gao, M.; Liu, Y.; Xian, K.; Peng, Z.; Zhou, K.; Liu, J.; Li, S.; Xie, F.; Zhao, W.; Zhang, J.; et al. Thermally stable poly(3-hexylthiophene): Nonfullerene solar cells with efficiency breaking 10%. *Aggregate* **2022**, e190. [CrossRef]
39. Liu, Y.; Xian, K.; Zhang, X.; Gao, M.; Shi, Y.; Zhou, K.; Deng, Y.; Hou, J.; Geng, Y.; Ye, L. A Mixed-Ligand Strategy to Modulate P3HT Regioregularity for High-Efficiency Solar Cells. *Macromolecules* **2022**, *55*, 3078–3086. [CrossRef]
40. Su, Y.; Zhang, L.; Ding, Z.; Zhang, Y.; Wu, Y.; Duan, Y.; Zhang, Q.; Zhang, J.; Han, Y.; Xu, Z.; et al. Carrier Generation Engineering toward 18% Efficiency Organic Solar Cells by Controlling Film Microstructure. *Adv. Energy Mater.* **2022**, *12*, 2103940. [CrossRef]
41. Gurney, R.S.; Li, W.; Yan, Y.; Liu, D.; Pearson, A.J.; Wang, T. Morphology and efficiency enhancements of PTB7-Th:ITIC nonfullerene organic solar cells processed via solvent vapor annealing. *J. Energy Chem.* **2019**, *37*, 148–156. [CrossRef]
42. Li, G.; Shrotriya, V.; Huang, J.; Yao, Y.; Moriarty, T.; Emery, K.; Yang, Y. High-efficiency solution processable polymer photovoltaic cells by self-organization of polymer blends. *Nat. Mater.* **2005**, *4*, 864–868. [CrossRef]
43. Liu, T.; Luo, Z.; Chen, Y.; Yang, T.; Xiao, Y.; Zhang, G.; Ma, R.; Lu, X.; Zhan, C.; Zhang, M.; et al. A nonfullerene acceptor with a 1000 nm absorption edge enables ternary organic solar cells with improved optical and mor-phological properties and efficiencies over 15%. *Energy Environ. Sci.* **2019**, *12*, 2529–2536. [CrossRef]
44. Tang, H.; Yan, C.; Huang, J.; Kan, Z.; Xiao, Z.; Sun, K.; Li, G.; Lu, S. Benzodithiophene-Based Small-Molecule Donors for Next-Generation All-Small-Molecule Organic Photovoltaics. *Matter* **2020**, *3*, 1403–1432. [CrossRef]
45. Liu, Q.; Jiang, Y.; Jin, K.; Qin, J.; Xu, J.; Li, W.; Xiong, J.; Liu, J.; Xiao, Z.; Sun, K.; et al. 18% Efficiency organic solar cells. *Sci. Bull.* **2020**, *65*, 272–275. [CrossRef]
46. Fan, Q.; Ma, R.; Liu, T.; Yu, J.; Xiao, Y.; Su, W.; Cai, G.; Li, Y.; Peng, W.; Guo, T.; et al. High-performance all-polymer solar cells enabled by a novel low bandgap non-fully conjugated polymer acceptor. *Sci. China Ser. B Chem.* **2021**, *64*, 1380–1388. [CrossRef]
47. Lin, Y.; Yu, L.; Xia, Y.; Firdaus, Y.; Dong, S.; Müller, C.; Inganäs, O.; Huang, F.; Anthopoulos, T.D.; Zhang, F.; et al. One-Step Blade-Coated Highly Efficient Nonfullerene Organic Solar Cells with a Self-Assembled Interfacial Layer Enabled by Solvent Vapor Annealing. *Sol. RRL* **2019**, *3*, 1900179. [CrossRef]
48. Liu, T.; Zhang, Y.; Shao, Y.; Ma, R.; Luo, Z.; Xiao, Y.; Yang, T.; Lu, X.; Yuan, Z.; Yan, H.; et al. Asymmetric Acceptors with Fluorine and Chlorine Substitution for Organic Solar Cells toward 16.83% Efficiency. *Adv. Funct. Mater.* **2020**, *30*, 2000456. [CrossRef]
49. Ma, R.; Zeng, M.; Li, Y.; Liu, T.; Luo, Z.; Xu, Y.; Li, P.; Zheng, N.; Li, J.; Li, Y.; et al. Rational Anode Engineering Enables Progresses for Different Types of Organic Solar Cells. *Adv. Energy Mater.* **2021**, *11*, 2100492. [CrossRef]
50. Yao, J.; Qiu, B.; Zhang, Z.-G.; Xue, L.; Wang, R.; Zhang, C.; Chen, S.; Zhou, Q.; Sun, C.; Yang, C.; et al. Cathode engineering with perylene-diimide interlayer enabling over 17% efficiency single-junction organic solar cells. *Nat. Commun.* **2020**, *11*, 2726. [CrossRef]
51. Liu, T.; Gao, W.; Wang, Y.; Yang, T.; Ma, R.; Zhang, G.; Zhong, C.; Ma, W.; Yan, H.; Yang, C. Unconjugated Side-Chain Engineering Enables Small Molecular Acceptors for Highly Efficient Non-Fullerene Organic Solar Cells: Insights into the Fi-ne-Tuning of Acceptor Properties and Micromorphology. *Adv. Funct. Mater.* **2019**, *29*, 1902155. [CrossRef]
52. Jiang, X.; Chotard, P.; Luo, K.; Eckmann, F.; Tu, S.; Reus, M.A.; Yin, S.; Reitenbach, J.; Weindl, C.L.; Schwartzkopf, M.; et al. Revealing Donor–Acceptor Interaction on the Printed Active Layer Morphology and the Formation Kinetics for Nonfullerene Organic Solar Cells at Ambient Conditions. *Adv. Energy Mater.* **2022**, *12*, 2103977. [CrossRef]
53. Müller-Buschbaum, P. The Active Layer Morphology of Organic Solar Cells Probed with Grazing Incidence Scattering Techniques. *Adv. Mater.* **2014**, *26*, 7692–7709. [CrossRef]
54. Luo, Z.; Liu, T.; Chen, Z.; Xiao, Y.; Zhang, G.; Huo, L.; Zhong, C.; Lu, X.; Yan, H.; Sun, Y.; et al. Isomerization of Perylene Diimide Based Acceptors Enabling High-Performance Nonfullerene Organic Solar Cells with Excellent Fill Factor. *Adv. Sci.* **2019**, *6*, 1802065. [CrossRef] [PubMed]
55. Ma, R.; Li, G.; Li, D.; Liu, T.; Luo, Z.; Zhang, G.; Zhang, M.; Wang, Z.; Luo, S.; Yang, T.; et al. Under-standing the Effect of End Group Halogenation in Tuning Miscibility and Morphology of High-Performance Small Molecular Acceptors. *Solar RRL* **2020**, *4*, 2000250. [CrossRef]

56. Liu, T.; Huo, L.; Chandrabose, S.; Chen, K.; Han, G.; Qi, F.; Meng, X.; Xie, D.; Ma, W.; Yi, Y.; et al. Optimized Fibril Network Morphology by Precise Side-Chain Engineering to Achieve High-Performance Bulk-Heterojunction Organic Solar Cells. *Adv. Mater.* **2018**, *30*, e1707353. [CrossRef]
57. Fu, J.; Chen, H.; Huang, P.; Yu, Q.; Tang, H.; Chen, S.; Jung, S.; Sun, K.; Yang, C.; Lu, S.; et al. Eutectic phase behavior induced by a simple additive contributes to efficient organic solar cells. *Nano Energy* **2021**, *84*, 105862. [CrossRef]
58. Ma, R.; Chen, Y.; Liu, T.; Xiao, Y.; Luo, Z.; Zhang, M.; Luo, S.; Lu, X.; Zhang, G.; Li, Y.; et al. Improving the performance of near infrared binary polymer solar cells by adding a second non-fullerene intermediate band-gap acceptor. *J. Mater. Chem. C* **2019**, *8*, 909–915. [CrossRef]
59. Ma, R.; Yan, C.; Yu, J.; Liu, T.; Liu, H.; Li, Y.; Chen, J.; Luo, Z.; Tang, B.; Lu, X.; et al. High-Efficiency Ternary Organic Solar Cells with a Good Figure-of-Merit Enabled by Two Low-Cost Donor Polymers. *ACS Energy Lett.* **2022**, *7*, 2547–2556. [CrossRef]